BIOLOGICAL CRYSTALLOGRAPHY

ISSN 1399-0047

Structure of the 34 kDa F-actin-bundling protein ABP34 from *Dictyostelium discoideum*

Min-Kyu Kim,‡§ Ji-Hye Kim,‡ Ji-Sun Kim‡ and Sa-Ouk Kang*

Laboratory of Biophysics, School of Biological Sciences, and Institute of Microbiology, Seoul National University, Seoul 151-742, Republic of Korea. *Correspondence e-mail: kangsaou@snu.ac.kr

Received 31 March 2015
Accepted 30 June 2015

Edited by M. Schiltz, Fonds National de la Recherche, Luxembourg

‡ These authors contributed equally to this work.
§ Present address: Biological Oceanography and Marine Biology Division, Korea Institute of Ocean Science and Technology, 787 Haean-ro(st), Ansan, Gyeonggi 426-744, Republic of Korea.

Keywords: EF-hand; F-actin bundling; ABP34; *Dictyostelium discoideum*; crystal structure.

PDB reference: 34 kDa F-actin-bundling protein, 4x3n

Supporting information: this article has supporting information at journals.iucr.org/d

The crystal structure of the 34 kDa F-actin-bundling protein ABP34 from *Dictyostelium discoideum* was solved by Ca^{2+}/S-SAD phasing and refined at 1.89 Å resolution. ABP34 is a calcium-regulated actin-binding protein that cross-links actin filaments into bundles. Its *in vitro* F-actin-binding and F-actin-bundling activities were confirmed by a co-sedimentation assay and transmission electron microscopy. The co-localization of ABP34 with actin in cells was also verified. ABP34 adopts a two-domain structure with an EF-hand-containing N-domain and an actin-binding C-domain, but has no reported overall structural homologues. The EF-hand is occupied by a calcium ion with a pentagonal bipyramidal coordination as in the canonical EF-hand. The C-domain structure resembles a three-helical bundle and superposes well onto the rod-shaped helical structures of some cytoskeletal proteins. Residues 216–244 in the C-domain form part of the strongest actin-binding sites (193–254) and exhibit a conserved sequence with the actin-binding region of α-actinin and ABP120. Furthermore, the second helical region of the C-domain is kinked by a proline break, offering a convex surface towards the solvent area which is implicated in actin binding. The F-actin-binding model suggests that ABP34 binds to the side of the actin filament and residues 216–244 fit into a pocket between actin subdomains −1 and −2 through hydrophobic interactions. These studies provide insights into the calcium coordination in the EF-hand and F-actin-binding site in the C-domain of ABP34, which are associated through interdomain interactions.

1. Introduction

Actin is one of the most highly conserved and abundant intracellular proteins in all eukaryotic cells, where it plays pivotal roles in contraction, cell shape, motility and subcellular organization. Actin is a member of a larger superfamily of proteins (Bork *et al.*, 1992; Kabsch & Holmes, 1995) which includes Hsp70 (Flaherty *et al.*, 1990), the cell-division protein FtsA (van den Ent & Löwe, 2000) and sugar kinases (Hurley *et al.*, 1993; Anderson *et al.*, 1978). Three-dimensional structures have revealed that members of the actin superfamily have the characteristic core of actin and are distinguished by additional insertions or deletions that are necessary for the specific function of each family member. In addition to the eukaryotic variants, the actin superfamily also encompasses members from both the bacterial and archaeal domains of life. Bacterial actin-like proteins include ParM plasmid-partitioning proteins (van den Ent *et al.*, 2002), MamK proteins involved in magnetosome organization (Komeili *et al.*, 2006), Hsp70 heat-shock proteins (Bork *et al.*, 1992) and a divergent family of actin-like proteins (ALPs) with largely unknown function (Derman *et al.*, 2009). MreB proteins are also prominent members of the bacterial actin family and have been shown to form spiral-shaped intracellular structures that play a key role in cell-shape determination (van den Ent *et al.*, 2001; Jones *et*

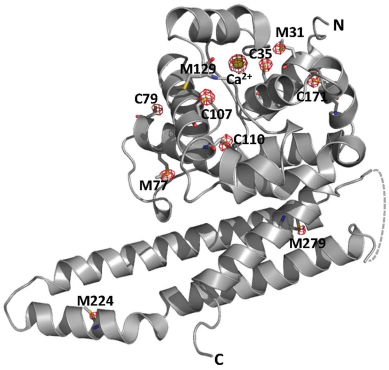

Table 1
Macromolecule-production information.

Source organism	*D. discoideum*
DNA source	cDNA
Gene sequence	ATGGCAGAAACAAAAGTTGCACCAAATCTTACTG- GTATTGAGCAAACCAAGGCAGGTCAATCCTTC- ACTGAAAAATTATCAGCTGAAGCTATGGAATT- TTTCTGTAATGTTGCCAAATTACCATTCTCAC- AACAAGCTGTTCACTTTTTGAATGCTTATTGG- GCTGAAGTTAGCAAAGAAGCTGAATTCATCTA- TTCCGTTGGTTGGGAAACAATCAAATATGCTG- ATATGCATTGCAAAGGTATCCAACTCGTTTTC- AAATACGATGAAGGTAACGATTTGGATTTCGA- TATTGCTCTCTATTTCTATGAACAATTATGCA- AATTCTGTGAAGATCCAAAGAACAAAAACTAT- GCAACCACCTACCCAATCTCTCAACCACAAAT- GTTGACTGCTCTCAAACGTAAACAAGAATTAA- GAGAAAAAGTCGATGTCAATTTCGATGGTCGT- GTCTCTTTCCTCGAATATCTCTTATATCAATA- CAAAGATTTCGCCAATCCAGCTGATTTCTGTA- CTCGTTCAATGAACCACGATGAACATCCAGAA- ATCAAAAAAGCTCGTTTAGCTCTCGAAGAAGT- CAACAAACGTATTCGTGCTTACGAAGAAGAAA- AAGCCCGTTTAACCGAAGAATCAAAGATTCCA- GGTGTCAAAGGTCTCGGTGCCACAAACATGCT- CGCTCAAATTGATAGTGGTCCATTAAAGGAAC- AACTCAACTTTGCCCTTATCTCTGCTGAAGCT- GCTGTTCGTACTGCTTCAAAGAAATATGGTGG- TGCTGCTTATTCAGGTGGTGCTGGTGATGCTG- GTGCTGGTTCCTCTGCTGGTGCCATTTGGTGG- ATGAATCGTGATTTAGAAGAAAAGAAAAAGAG- ATACGGTCCACAAAAGAAATAA
Forward primer (5′→3′)†	5′-CATATGGCAGAAACAAAAGTTGCA-3′
Reverse primer (5′→3′)‡	5′-GGATCCTTATTTCTTTTGTGGACCGTA-3′
Cloning vector	pGEM-T
Expression vector	pET-3a
Expression host	*E. coli* BL21 (DE3)
Complete amino-acid sequence of the construct produced	MAETKVAPNLTGIEQTKAGQSFTEKLSAEAMEFF- CNVAKLPFSQQAVHFLNAYWAEVSKEAEFIYS- VGWETIKYADMHCKGIQLVFKYDEGNDLDFDI- ALYFYEQLCKFCEDPKNKNYATTYPISQPQML- TALKRKQELREKVDVNFDGRVSFLEYLLYQYK- DFANPADFCTRSMNHDEHPEIKKARLALEEVN- KRIRAYEEEKARLTEESKIPGVKGLGATNMLA- QIDSGPLKEQLNFALISAEAAVRTASKKYGGA- AYSGGAGDAGAGSSAGAIWWMNRDLEEKKKRY- GPQKK

† The NdeI site is underlined. ‡ The BamHI site is underlined.

al., 1991). Crenactin is an actin homologue that is unique to the archaeal kingdom Crenarchaeota and has the highest sequence similarity to eukaryotic actin of any known actin homologue (Ettema *et al.*, 2011; Lindås *et al.*, 2014).

Actin is found in two forms, namely monomeric G-actin and filamentous F-actin. *In vitro*, ATP-bound G-actin polymerizes in the presence of cations (K^+ and Mg^{2+}) and this reaction is followed by the hydrolysis of ATP to ADP. In a cell, a dense meshwork of F-actin is closely associated with the plasma membrane. This so-called actin cortex plays an important role in the maintenance and control of the cell shape and architecture. The dynamic remodelling of the actin cytoskeleton is essential for migration, cytokinesis, endocytosis and a range of morphological and developmental programmes. These processes rely on the coordination of signalling pathways that regulate the site and timing of filament (F-actin) assembly as well as the organization of individual filaments into higher-order structures. The precise spatial and temporal control of the assembly, disassembly and contractility of the actin cytoskeleton is important in a cell. The dynamic assembly/disassembly of the actin cytoskeleton is regulated by a large number of actin-interacting proteins, particularly cross-linking and bundling proteins. Several hundred actin-binding proteins (ABPs) interact with different protein motifs to control both the G-actin- and F-actin-modulating actin-polymerization rates, the intracellular localization of actin polymers and the structural and functional properties of different actin-filament variants (Goodson & Hawse, 2002; Vorobiev *et al.*, 2003). In particular, F-actin-bundling proteins play an essential role in the regulation of cell structure and motility because they participate in the rearrangement and localization of actin filaments through the formation and stabilization of actin bundles and three-dimensional networks (Furukawa & Fechheimer, 1997; Matsudaira, 1991; Otto, 1994).

To date, 11 different actin cross-linking proteins have been identified in *Dictyostelium* (Furukawa & Fechheimer, 1997), which has been a model system for the analysis of many of the underlying actin-driven processes, and research in this field has contributed to a general understanding of the structure and function of cytoskeletal proteins (Noegel & Luna, 1995; Schleicher & Noegel, 1992). Among them, ABP34 is one of the two calcium-regulated proteins that function primarily to induce the formation of actin-filament bundles in a calcium-regulated manner (Fechheimer & Taylor, 1984; Prassler *et al.*, 1997). ABP34 has been localized to the cell cortex, filopodia, pseudopodia, cleavage furrow and phagocytic cup (Fechheimer, 1987; Furukawa *et al.*, 1992; Furukawa & Fechheimer, 1994; Okazaki & Yumura, 1995). Furthermore, ABP34 stabilizes the membrane-associated actin-based cytoskeleton in cell–cell contact sites (Fechheimer *et al.*, 1994). Calcium is a prominent regulator that can exert multiple effects on the structure and dynamics of the actin cytoskeleton (Furukawa *et al.*, 2003; Lee *et al.*, 2005). *In vitro* studies have shown that ABP34 has one high-affinity calcium-binding site, which resides in the putative EF-hand. ABP34 bundles actin at low calcium ($1 \times 10^{-8}\ M$), but at elevated calcium levels ($1 \times 10^{-6}\ M$) the protein is unable to bundle F-actin (Fechheimer, 1987; Fechheimer & Taylor, 1984; Lim & Fechheimer, 1997). *Dictyostelium* cells that are mutated in the calcium-binding EF-hand of ABP34 exhibit defects in the distribution of ABP34 and actin as well as in cell size and growth (Furukawa *et al.*, 2003).

Biochemical analyses using various truncation mutants of ABP34 indicates that it has three F-actin-binding sites and intramolecular interaction zones that are important for the regulation of actin binding (Lim, Furukawa, Eagle *et al.*, 1999; Lim, Furukawa & Fechheimer, 1999). ABP34 does not contain a calponin-homology (CH) domain, which is one of the most abundant actin-binding motifs (Broderick & Winder, 2005; Gimona *et al.*, 2002), but possesses a strong actin-binding site (193–254) and two weaker binding sites. In addition, the intramolecular interaction between interaction zone 1 (IZ-1; 71–123) and interaction zone 2 (IZ-2; 193–254) has been proposed to maintain the N-terminal region (1–76) in close proximity to the strong actin-binding site (193–254) to

Table 2
Crystallization.

Method	Hanging-drop vapour diffusion
Plate type	24-well
Temperature (K)	295
Protein concentration (mg ml^{-1})	30
Buffer composition of protein solution	10 m*M* HEPES pH 7.4, 0.1 *M* NaCl, 0.1 m*M* EGTA
Composition of reservoir solution	0.2 *M* ammonium acetate, 0.1 *M* sodium citrate pH 5.6, 30% PEG 4K
Volume and ratio of drop	2 µl, 1:1
Volume of reservoir (µl)	350

modulate the interaction of ABP34 with F-actin (Lim, Furukawa & Fechheimer, 1999). As a first step towards the elucidation of the detailed F-actin-bundling mechanisms of ABP34, in this study we report the crystal structure of calcium-bound ABP34 at 1.89 Å resolution. Moreover, *in vitro* and *in vivo* F-actin-bundling activity of ABP34 was also verified. Structural analyses revealed the calcium coordination in the EF-hand, interdomain interactions and a strong actin-binding site in a three-helical bundle of the C-domain.

2. Materials and methods

2.1. Cloning, expression and purification of ABP34

The full-length *abpB* gene (NCBI reference sequence XM_636770) coding for ABP34 was amplified by PCR using *D. discoideum* cDNA as a template. The amplified gene was inserted downstream of the T7 promoter of the expression plasmid pET-3a (Novagen), and the resulting construct expressed residues 1–295 of the ABP34 protein without any additional residues. After verifying the DNA sequence, the plasmid DNA was transformed into *Escherichia coli* BL21 (DE3) cells (Novagen) (Table 1). The cells were grown to an OD_{600} of approximately 0.5 in Luria–Bertani medium containing 0.1 mg ml^{-1} ampicillin and 34 µg ml^{-1} chloramphenicol at 37°C and expression was induced with 1 m*M* isopropyl *β*-D-1-thiogalactopyranoside (IPTG; Duchefa). After 12 h of induction at 22°C, the cells were harvested and resuspended in buffer *A* (100 m*M* HEPES pH 7.4) containing 1 m*M* phenylmethylsulfonyl fluoride (PMSF). The cells were disrupted by sonication and the cell debris was discarded by centrifugation at 20 000*g* for 30 min. The supernatant was loaded onto a DEAE Sepharose CL-6B (GE Healthcare) column and the ABP34-containing flowthrough was collected in buffer *A*. The protein solution was loaded onto a Superdex 75 HR 16/60 column (GE Healthcare) pre-equilibrated with 10 m*M* HEPES pH 7.4 containing 100 m*M* NaCl and 0.1 m*M* EGTA. The purified ABP34 was concentrated to approximately 30 mg ml^{-1} for crystallization (Table 2).

2.2. Crystallization and data collection

Crystal screening was conducted by the hanging-drop vapour-diffusion method using screening solutions available from Hampton Research and Emerald Bio. Droplets composed of 1 µl protein solution and an equal volume of crystallization screening solution were equilibrated against 350 µl reservoir solution at 22°C. Rhombus-shaped crystals were produced using 0.2 *M* ammonium acetate, 0.1 *M* sodium citrate pH 5.6, 30% PEG 4K after 3 d. The initial crystallization conditions were optimized by modifying the buffer pH, salt content and PEG concentration. Single crystals of ABP34 were mounted using a nylon loop (50 µm Mounted CryoLoop, Hampton Research) for data collection and were cooled to 100 K using a Cryostream cooler (Oxford Cryosystems) without additional cryoprotectant. A 1.89 Å resolution native data set was collected at a wavelength of 1.1 Å using an ADSC Quantum 210 CCD on beamline 6C at Pohang Light Source (PLS), Republic of Korea. A total of 360 frames of 1° oscillation were collected with the crystal-to-detector distance set to 150 mm (Table 1). A 2.30 Å resolution SAD data set was collected at a wavelength of 1.9 Å using an ADSC Quantum 270 CCD on beamline 7A of PLS, Republic of Korea. A total of 999 frames of 1° oscillation were collected with the crystal-to-detector distance set to 120 mm (Table 3).

Table 3
Data collection and processing.

Values in parentheses are for the outer shell.

	Ca^{2+}/S-SAD	Native
Diffraction source	BL-7A, PLS	BL-6C, PLS
Wavelength (Å)	1.9075	1.1000
Temperature (K)	100	100
Detector	ADSC Quantum 270 CCD	ADSC Quantum 210 CCD
Crystal-to-detector distance (mm)	120	150
Rotation range per image (°)	1	1
Total rotation range (°)	999	360
Exposure time per image (s)	1	2
Space group	$P2_12_12_1$	$P2_12_12_1$
a, *b*, *c* (Å)	78.878, 85.902, 136.891	78.161, 85.244, 135.744
α, *β*, *γ* (°)	90, 90, 90	90, 90, 90
Mosaicity (°)	0.300	0.472
Resolution range (Å)	50.00–2.30 (2.34–2.30)	50.00–1.89 (1.93–1.89)
Total No. of reflections	1005649	696218
No. of unique reflections	40890	72226
Completeness (%)	96.9 (87.8)	98.9 (88.2)
Multiplicity	24.6 (11.1)	9.6 (5.4)
$\langle I/\sigma(I)\rangle$	58.7 (4.3)	32.5 (2.9)
$R_{\rm r.i.m.}$† (%)	6.6 (40.5)	8.2 (46.4)
Overall *B* factor from Wilson plot (Å^2)	33.6	21.9

† $R_{\rm r.i.m.}$ was estimated by multiplying the conventional $R_{\rm merge}$ value by the factor $[N/(N-1)]^{1/2}$, where N is the data multiplicity.

2.3. Data processing, structure determination and refinement

The diffraction data were processed and scaled using *DENZO* and *SCALEPACK* from the *HKL*-2000 program suite (Otwinowski & Minor, 1997). The structure was determined by the Ca^{2+}/S single-wavelength anomalous dispersion (SAD) phasing method. SAD phasing was performed with the *AutoSol* program (Terwilliger *et al.*, 2009) in the *PHENIX* suite (Adams *et al.*, 2010), which is an experimental phasing pipeline that combines *HySS* (*Hybrid Substructure Search*; Grosse-Kunstleve & Adams, 2003) for finding heavy-atom sites, *Phaser* (McCoy *et al.*, 2007) or *SOLVE* (Terwilliger, 2002) for calculating experimental phases and *RESOLVE*

Table 4
Structure solution and refinement.

Values in parentheses are for the outer shell.

Resolution range (Å)	72.19–1.89 (1.94–1.89)
Completeness (%)	99.2 (94.6)
No. of reflections, working set	68586
No. of reflections, test set	3640
Final R_{cryst} (%)	21.8
Final R_{free} (%)	25.5
Cruickshank DPI	0.167
No. of non-H atoms	
Protein	6282
Calcium	3
Citrate	13
Water	383
Total	6681
R.m.s. deviations	
Bonds (Å)	0.009
Angles (°)	1.413
Average *B* factors (Å^2)	
Protein	34.0
Calcium	28.4
Citrate	50.6
Water	32.6
Ramachandran plot	
Most favoured (%)	97.2
Allowed (%)	2.5

(Terwilliger, 2002) for density modification and model building. The autobuilt models from the phasing programs were completed using *Coot* (Emsley & Cowtan, 2004) and refinement was performed with a maximum-likelihood algorithm implemented in *REFMAC*5 (Murshudov *et al.*, 2011) (Table 4). All figures showing structures were prepared with *PyMOL* (http://www.pymol.org).

2.4. F-actin co-sedimentation assay

Co-sedimentation assays were performed as described previously (Lim, Furukawa & Fechheimer, 1999). Actin from rabbit muscle (Sigma) was polymerized by the addition of polymerization buffer (20 m*M* PIPES pH 7.0, 50 m*M* KCl, 1 m*M* $MgCl_2$, 1 m*M* ATP, 1 m*M* DTT) containing 5 m*M* EGTA for 1 h at room temperature (25°C). The ABP34 protein (0.25 µ*M*) was mixed with prepared F-actin (5 µ*M*) under actin-polymerization conditions (20 m*M* PIPES pH 7.0, 50 m*M* KCl, 1 m*M* $MgCl_2$, 1 m*M* ATP, 5 m*M* EGTA, 0.25 m*M* $CaCl_2$ for low-Ca^{2+} conditions) for 24 h at 4°C and centrifuged in an ultracentrifuge (Beckman) at 115 000*g* for 1 h. Supernatant and pellet samples were collected and analyzed by 12% SDS–PAGE. The gel was visualized by Coomassie Brilliant Blue staining.

2.5. Cell culture and imaging

Axenic parental strain KAx3 cells were grown in HL5 medium, which was supplemented with 200 µg ml^{-1} streptomycin sulfate and 200 U ml^{-1} penicillin and shaken at 150 rev min^{-1} and 22°C. Constructs for GFP-fused ABP34 were introduced into *D. discoideum* KAx3 cells by electroporation. The transformants were selected using HL5 medium containing G418 (20 µg ml^{-1}) on tissue-culture plates. The expression vector for ABP34 was constructed by PCR using cDNA from *Dictyostelium* as a template and P1 (5′-GGATCCATGGCAGAAACAAAAGTTGCAC-3′) and P2 (5′-CTCGAGTTATTTCTTTTGTGGACCGTATCTC-3′) as primers. The PCR product was cloned into pGEM-T Easy vector (Promega) and cut by BamHI and XhoI. The resultant fragment was ligated into pTX-GFP vector for the construction of a green fluorescent protein (GFP) fusion with ABP34. After selection, cells overexpressing GFP-fused ABP34 were used for subcellular localization. Log-phase cells grown in suspension were diluted to a density of 2.5×10^6 cells ml^{-1} with HL5 and then fixed on cover slips with cold methanol containing 1% formaldehyde at −20°C for 5 min. To stain F-actin, the cells were incubated with 3 µg ml^{-1} tetramethylrhodamine-5-isothiocyanate (TRITC)-conjugated phalloidin (Sigma) for 1 h and washed three times with PBS. Cells were observed using a multi-photon confocal laser scanning microscope (DE/LSM510 NLO; Carl Zeiss) as described previously (Kim *et al.*, 2011).

2.6. Oligomeric state determination

170 µ*M* purified ABP34 and molecular-mass standards (Sigma) were applied onto a Superose 6 10/300 GL column (GE Healthcare) pre-equilibrated with 10 m*M* HEPES pH 7.4 containing 100 m*M* NaCl. A standard curve was generated by plotting the logarithm of the molecular mass of the standard proteins against their K_{av}, which was calculated using the equation $K_{av} = (V_e - V_0)/(V_t - V_0)$, where V_e is the elution volume, V_0 is the void volume and V_t is the total bed volume. The K_{av} of ABP34 determined using the same column was compared with the profile of the protein standards bovine serum albumin (66 kDa), carbonic anhydrase (29 kDa), cytochrome *c* (12.4 kDa) and aprotinin (6.5 kDa). All samples were allowed to equilibrate at room temperature (25°C) for at least 2 h before use. The calibration curves for the protein standards were determined by linear-squares analysis of the K_{av} as a function of log(molecular weight). The apparent molecular weight of native ABP34 was estimated to be 32 836 Da, showing that ABP34 behaves as a monomer.

2.7. Transmission electron microscopy

The actin filaments and bundles were visualized using an energy-filtering transmission electron microscope (LIBRA 120; Carl Zeiss, Germany) operated at an accelerating voltage of 120 kV. Actin (5 µ*M*) was polymerized in F-actin buffer consisting of 20 m*M* PIPES pH 7.0, 50 m*M* KCl, 1 m*M* $MgCl_2$, 1 m*M* ATP. F-actin (5 µ*M*) and ABP34 (1 µ*M*) were mixed in a buffer consisting of 0.25 m*M* $CaCl_2$, 5 m*M* EGTA and incubated overnight on ice. Samples (10 µl) of the resulting F-actin preparation mixtures were adsorbed onto carbon-coated copper grids (200 mesh) for 1 min, washed with F-actin buffer for 30 s, negatively stained with 2% uranyl acetate (Electron Microscopy Sciences, Hatfield, Pennsylvania, USA) for 1 min and air-dried. All types of images were recorded with a slow-scan charge-coupled device camera (Ultrascan 4000 SP; Gatan, Pleasanton, California, USA).

2.8. PDB code

The atomic coordinates and structure factors were deposited in the PDB with accession code 4x3n.

3. Results and discussion

3.1. Purification, characterization and crystallization of ABP34

ABP34 is a protein of 295 residues (calculated molecular weight of 33 352 Da) with an EF-hand motif in the N-domain and a strong actin-binding site in the C-domain. The deduced amino-acid sequence of ABP34 from *Dictyostelium* revealed homologues in some species of amoeba (Supplementary Fig. S1), but no sequence homology to other actin-binding proteins (Fechheimer & Furukawa, 1991). A few antigenic homologues of ABP34 have been identified in *Drosophila*, *Schistosoma* and mammalian cells (Johns *et al.*, 1988; Furukawa & Fechheimer, 1990). To elucidate its structural and biochemical properties, we first subcloned, expressed and purified full-length (1–295) wild-type recombinant ABP34 (Fig. 1*a*). The molecular mass determined by gel filtration was 32 836 Da, which is close to the theoretical mass of 33 352 Da, indicating that ABP34 is monomeric (Figs. 1*b* and 1*c*), in agreement with previous reports (Fechheimer & Taylor, 1984; Lim, Furukawa, Eagle *et al.*, 1999). Various buffer conditions (buffer components, pH, salt concentration *etc.*) were tested, but these did not significantly affect the oligomeric state of ABP34 (data not shown). The far-UV CD spectrum of wild-type ABP34 has the characteristic minima at 210 and 220 nm showing that the protein has a high content of α-helical secondary structure (Supplementary Fig. S2). Free calcium ion in the concentration range 0–5 m*M* does not influence the secondary structure of ABP34. The addition of 5 m*M* EGTA also has no effect on the conformation of ABP34. These results suggest that (i) the calcium-binding site is not exposed to the surface region and/

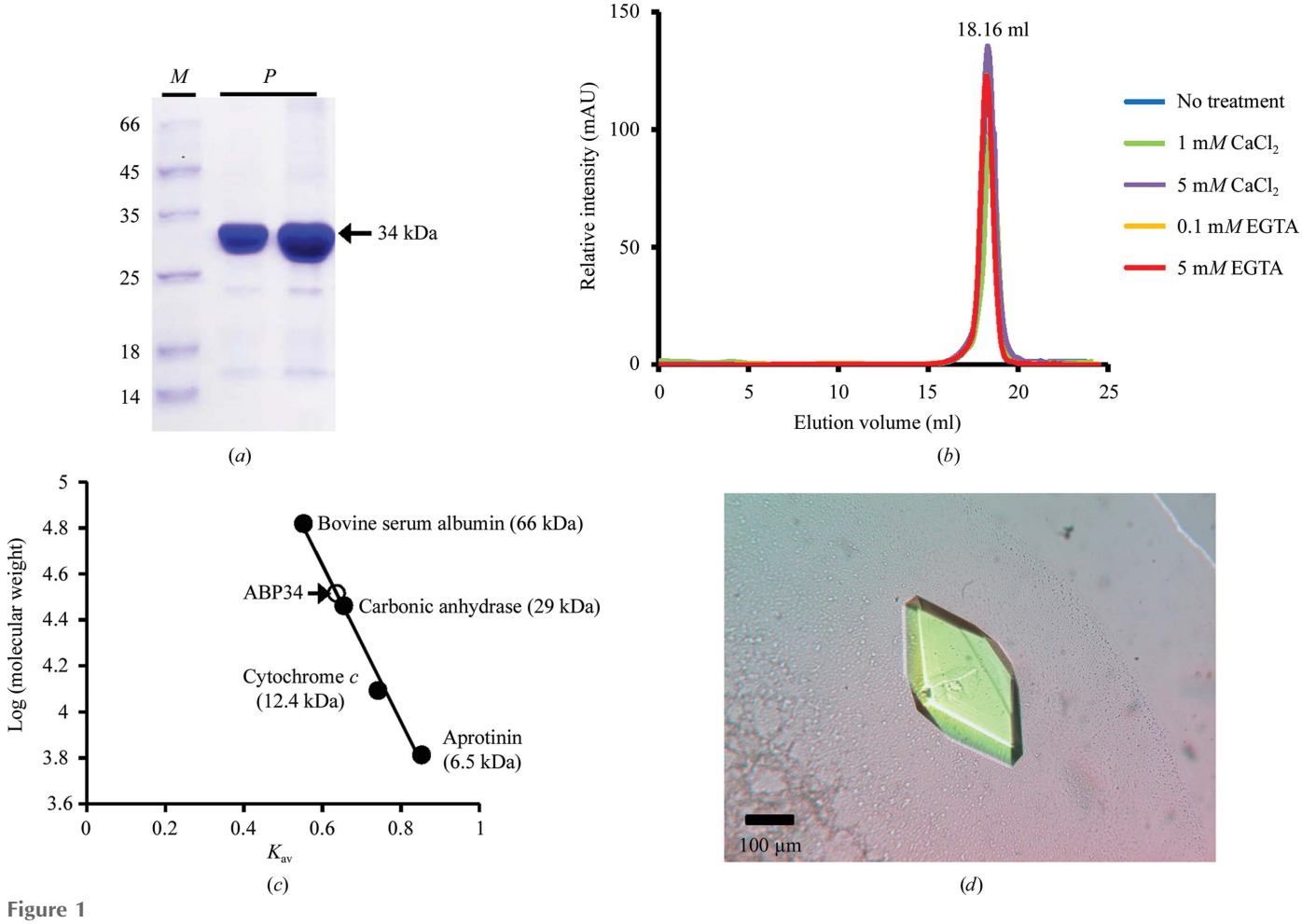

Figure 1
Purification and crystallization of ABP34. (*a*) SDS–PAGE analysis of the purified ABP34 used for crystallization and analytical gel filtration. The gel was stained using Coomassie Brilliant Blue. Lane *P*, 30 µg purified ABP34; lane *M*, molecular-weight markers (labelled in kDa). (*b*) Analytical gel-filtration profile of ABP34. 170 µ*M* purified ABP34 was applied onto a Superose 6 10/300 GL size-exclusion column. The ABP34 peak eluted 18.16 ml after injection. Elution peaks were detected in the presence of 1 m*M* $CaCl_2$, 5 m*M* $CaCl_2$, 0.1 m*M* EGTA and 5 m*M* EGTA, respectively, in buffer consisting of 10 m*M* HEPES pH 7.4, 100 m*M* NaCl. The concentration of ABP34 was approximately 10 µ*M* for each elution peak. (*c*) Standard curve of analytical gel filtration generated with molecular-weight markers (bovine serum albumin, 66 kDa; carbonic anhydrase, 29 kDa; cytochrome *c*, 12.4 kDa; aprotinin, 6.5 kDa). The positions of the molecular-weight markers are indicated by black dots. The position of ABP34 is marked by a white dot. (*d*) Rhombus-shaped single crystal of ABP34.

or (ii) the EF-hand has a high affinity for calcium ions and is already occupied by a calcium ion. Because ABP34 bundles F-actin in a calcium-regulated manner, comparison of the structural differences between the Ca^{2+}-free and Ca^{2+}-bound states of ABP34 is essential. To solve the high-resolution crystal structure of ABP34, 30 mg ml^{-1} purified recombinant ABP34 was used for crystallization. Crystal screening was conducted by the hanging-drop vapour-diffusion method and rhombus-shaped single crystals were produced using a solution consisting of 0.2 *M* ammonium acetate, 0.1 *M* sodium citrate pH 5.6, 30% PEG 4K (Fig. 1*d*).

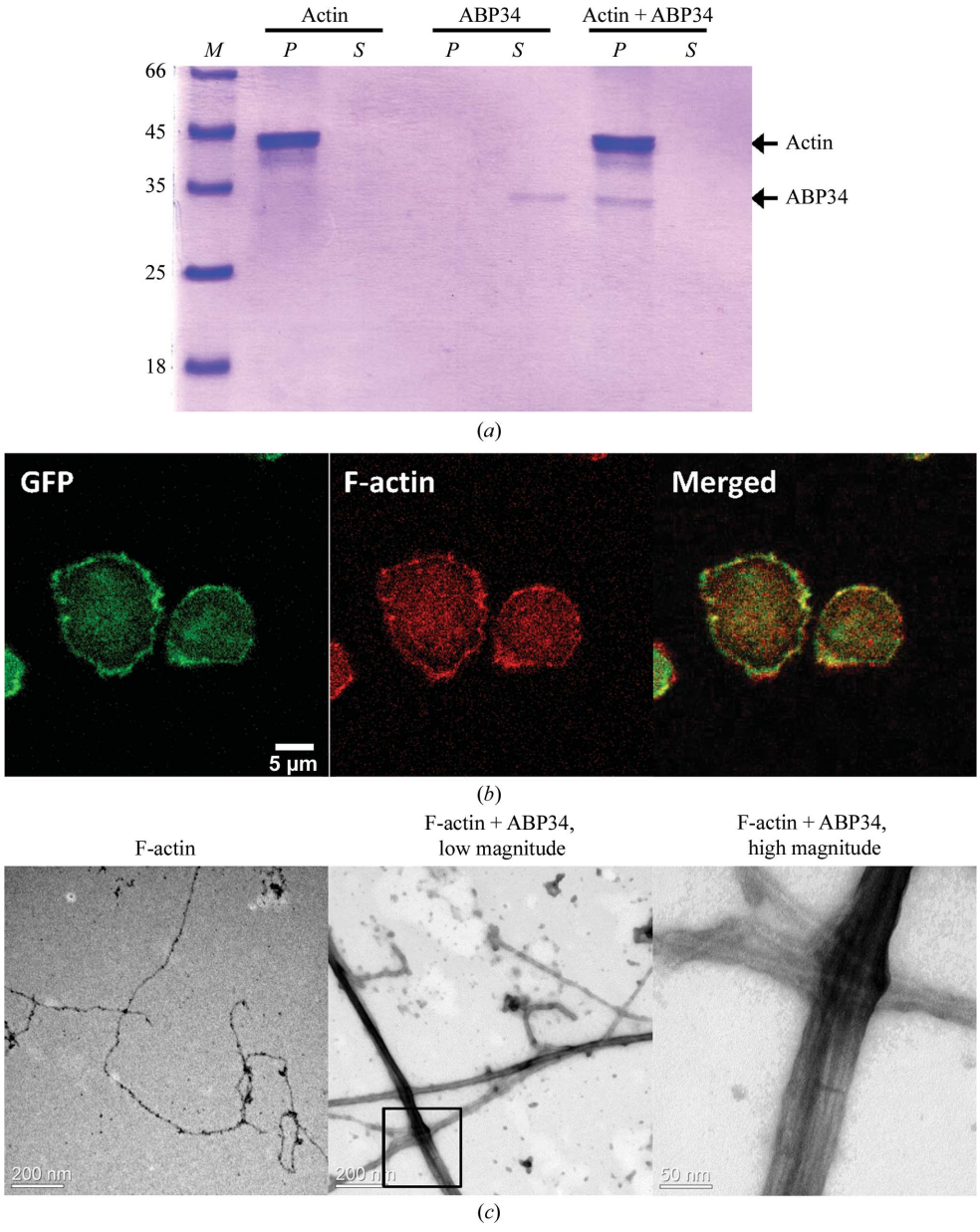

Figure 2
Actin-binding and actin-bundling activities of ABP34. (*a*) Binding of ABP34 to F-actin in solution. F-actin co-sedimentation assays were analyzed by Coomassie Brilliant Blue-stained 12% SDS–PAGE. Lane *M*, molecular-weight markers (labelled in kDa). In the other lanes, *S* and *P* indicate supernatant and pellet fractions of F-actin co-sedimentation assays, respectively. In the actin-binding co-sedimentation assays with ABP34, 5 µ*M* actin and 0.25 µ*M* ABP34 were used. ABP34, which bound strongly to F-actin in solution, was found with F-actin in the pellet. (*b*) Distribution of F-actin and ABP34 *in vivo*. The cells expressing GFP-ABP34 were placed on a glass cover slip in nutrient medium, allowed to adhere, fixed with cold methanol and stained for F-actin with TRITC-conjugated phalloidin (middle). Images of *Dictyostelium* cells expressing GFP-ABP34 were recorded with a multi-photon confocal laser scanning microscope. GFP-ABP34-expressing cells (left) exhibited a high concentration of GFP-ABP34 in the cortical region along with F-actin according to the merged image (right). The scale bar represents 5 µm. (*c*) Transmission electron micrographs of the F-actin and ABP34 mixture in buffer consisting of 20 m*M* PIPES pH 7.0, 50 m*M* KCl, 1 m*M* $MgCl_2$, 1 m*M* ATP, 5 m*M* EGTA, 0.25 m*M* $CaCl_2$. Left, 5 µ*M* F-actin; middle, 5 µ*M* F-actin with 1 µ*M* ABP34 (low magnitude); right, 5 µ*M* F-actin with 1 µ*M* ABP34 (high magnitude). F-actin bundles are formed in the presence of ABP34 (middle, right). Scale bars represent 200 nm (left and middle) and 50 nm (right).

3.2. Actin binding of ABP34

The F-actin-binding and F-actin-bundling activities were determined by a high-speed co-sedimentation assay and transmission electron microscopy of negatively stained F-actin. The co-sedimentation assay was performed as previously established (Lim & Fechheimer, 1997; Fechheimer, 1987). A molar ratio of 20:1 F-actin:ABP34 was used under low free-calcium concentration conditions (Fechheimer & Taylor, 1984). The mixture was separated into supernatant and pellet fractions by high-speed centrifugation. Proteins that bound strongly to F-actin in solution were found with F-actin in the pellet. In the absence of F-actin, ABP34 remained in the supernatant. However, in the presence of F-actin the ABP34 protein was found with F-actin in the pellet, indicating that ABP34 binds tightly to F-actin (Fig. 2*a*). The localization of ABP34 and F-actin was also observed in the cell by fluorescence microscopy. GFP-ABP34 was expressed in *D. discoideum* cells (Supplementary Fig. S3) and F-actin was stained with TRITC-conjugated phalloidin. As shown in Fig. 2(*b*), ABP34 and actin filaments were co-localized in the cell cortex of a single cell. The association of ABP34 with F-actin suggests the ability of ABP34 to bind F-actin *in vivo*.

The F-actin-bundling ability of ABP34 was examined by

transmission electron microscopy after negative staining. To generate a cross-linked structure of ABP34 and F-actin, the reaction mixtures of ABP34 and F-actin were incubated with 0.25 m*M* $CaCl_2$, 5 m*M* EGTA overnight on ice. The concentrations of F-actin and ABP34 used were 5 and 1 µ*M*, respectively. The electron microscope showed that mixtures of ABP34 and F-actin contained large actin bundles (Fig. 2*c*). These structures were not formed when actin filaments were used alone. Upon further examination at higher magnification, it is clear that bundling of F-actin was obtained through the interaction of ABP34 with actin. These data demonstrate that ABP34 generates highly ordered actin bundles that contain several folds of parallel actin filaments.

3.3. Calcium/sulfur SAD phasing

To determine the crystal structure of ABP34, we attempted to perform molecular replacement (MR) and experimental phasing using selenium multiwavelength anomalous dispersion (Se-MAD). However, all of the trials failed owing to the lack of a proper search model in the PDB for MR or the poor diffraction quality of the selenomethionine-derivative crystals for Se-MAD. Finally, motivated by the presence of five cysteines and seven methionines in the ABP34 monomer, sulfur SAD (S-SAD) phasing was attempted based on the anomalous signal of sulfur. A 2.3 Å resolution SAD data set (Table 3) was collected at a wavelength of 1.9 Å. The crystal of ABP34 belonged to the orthorhombic space group $P2_12_12_1$, with unit-cell parameters $a = 78.878$, $b = 85.902$, $c = 136.891$ Å. There are three molecules in the asymmetric unit, giving a Matthews coefficient (V_M) of 2.28 $Å^3$ Da^{-1} (Matthews, 1968) and a calculated solvent content of 46.14%. Anomalous signals, which were evaluated by $\langle d''/\text{sig}\rangle$, a good indicator of the strength of the anomalous signal, were above the threshold (0.80; Sheldrick, 2010) to the highest resolution shell (Fig. 3*a*). S-SAD phasing generally requires highly redundant data to accurately measure the subtle anomalous signal. Therefore, we rescaled the SAD data set in a total 999 frames to evaluate the effect of multiplicity (Fig. 3*a*). Despite the presence of a reasonable anomalous signal, an interpretable electron-density map can be calculated from data frames 1–500 (data not shown).

The *AutoSol* program was used to find anomalous sulfur substructures and produced a phase set with figures of merit (FOMs) before and after density modification of 0.30 and 0.65, respectively. In fact, among the 34 heavy-atom sites found by *HySS*, three sites turned out to be the calcium ions occupying the calcium-binding EF-hand motif of the N-domain (Fig. 3*b*). The lower occupancy of sulfur positions is an expression of the smaller dispersive signal of sulfur compared with calcium ($f'' = 0.82\ e^-$ *versus* $f'' = 1.84\ e^-$) at the wavelength of 1.9 Å. Although the location of the Ca atoms, which are relatively strong anomalous scatterers ($f'' = 1.84\ e^-$), may facilitate the finding of S atoms ($f'' = 0.82\ e^-$), the data evidently contained a meaningful anomalous scattering contribution originating from sulfur as in previous successful cases of Ca^{2+}/S-SAD phasing (Roeser *et al.*, 2005; Koch *et al.*, 2010). This result is also in accordance with the report that the location of Mn atoms facilitates the finding of S atoms and that the anomalous scattering of S atoms contributes to SAD phasing (Ramagopal *et al.*, 2003). The experimental electron-density map was clearly interpretable and a model consisting of 749 residues out of the total 885 amino acids with an R_{work} and an R_{free} of 0.236 and 0.288, respectively, was automatically built. The final model with an R_{work} and an R_{free} of 0.218 and 0.255, respectively, was built manually using *Coot* (Emsley & Cowtan, 2004) with the 1.89 Å resolution native data set, and iterative rounds of refinement were performed using *REFMAC*5 (Murshudov *et al.*, 2011) (Table 4).

3.4. Overall structure of ABP34

As a first step towards verifying the mechanism of F-actin bundling by ABP34, we determined the crystal structure of

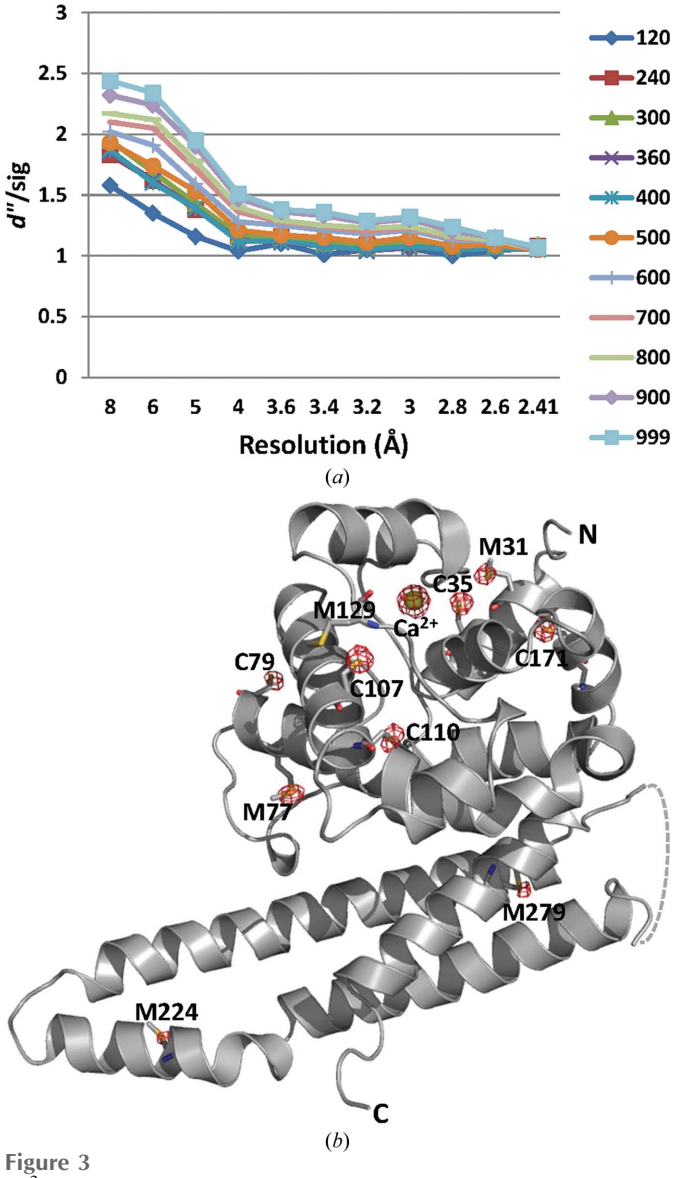

Figure 3
Ca^{2+}/S-SAD phasing. (*a*) The $\langle d''/\text{sig}\rangle$ plots from *SHELXC* as a function of resolution. (*b*) Anomalous Fourier maps (red mesh) at the 5σ level. The calcium ion and the S atoms from cysteine and methionine are represented by a yellow sphere and yellow sticks, respectively.

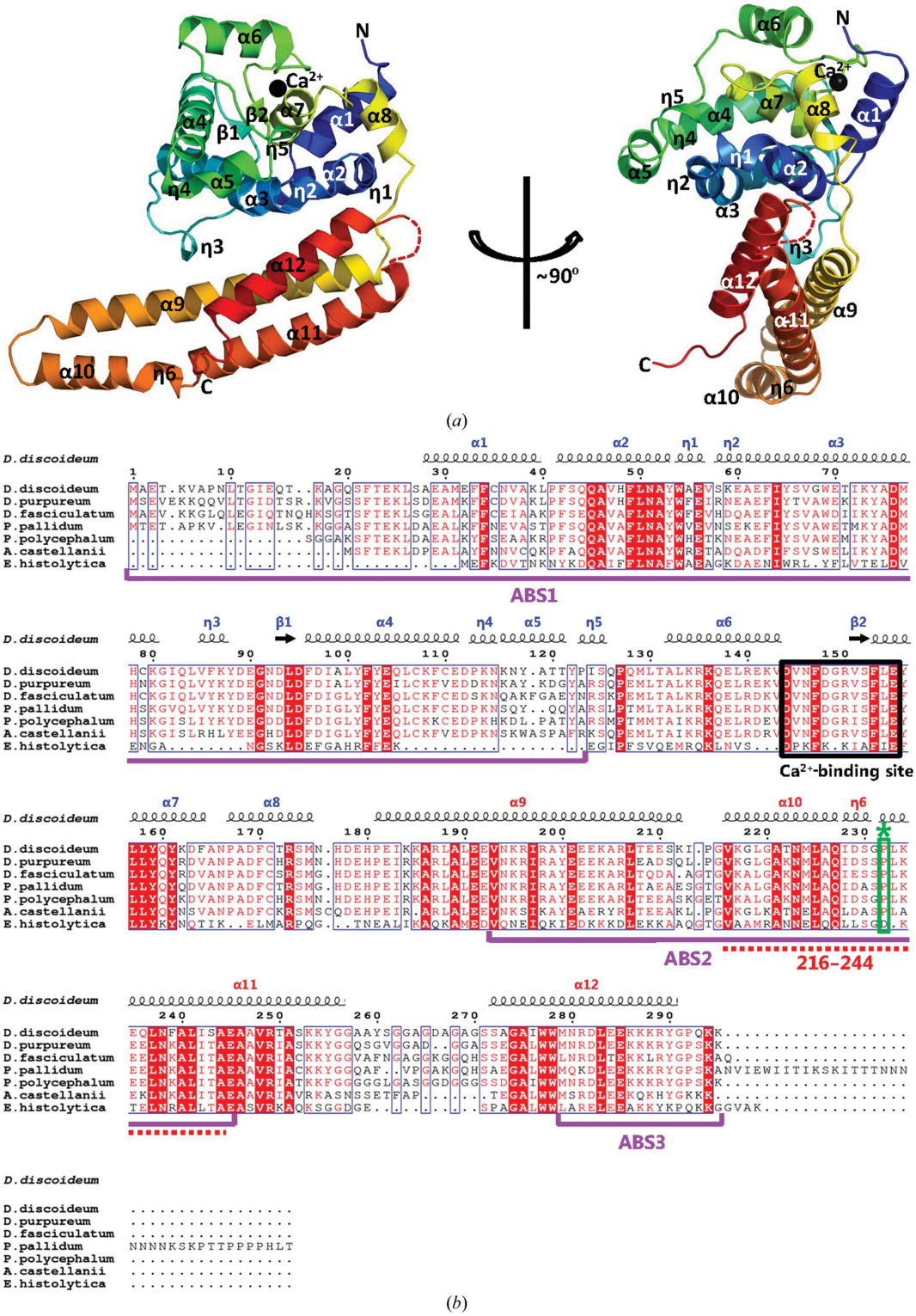

Figure 4
Overall structure of ABP34. (*a*) Cartoon representation of the ABP34 monomer structure from front (left) and side (right) views. The molecule is coloured progressively from blue at the N-terminus to red at the C-terminus. Secondary structures including helices and sheets are labelled. The calcium ion is highlighted with a black sphere and the disordered region (257–269) is shown as a dotted line. (*b*) Structure-based multiple sequence alignment of ABP34 with the homologues from amoebal species. The secondary-structure elements of *D. discoideum* ABP34 are shown above the alignment (N-domain; blue, C-domain; red). Homologous regions are boxed, with identical amino-acid residues shown as bold white letters on a red background and functionally equivalent residues shown as red letters. Residues in the Ca^{2+}-binding site are highlighted with black boxes and the conserved actin-binding residues are indicated by red dots. The proposed actin-binding sites ABS1, ABS2 and ABS3 are underlined in magenta and the proline kink is marked with an green asterisk and boxed in green. The full names of the strains are as follows: *D. purpureum*, *Dictyostelium purpureum*; *D. fasciculatum*, *Dictyostelium fasciculatum*; *P. pallidum*, *Polysphondylium pallidum*; *P. polycephalum*, *Physarum polycephalum*; *A. castellanii*, *Acanthamoeba castellanii*; *E. histolytica*, *Entamoeba histolytica*.

ABP34. ABP34 from *D. discoideum* was crystallized in the orthorhombic space group $P2_12_12_1$. The crystal structure of ABP34 was determined by Ca^{2+}/S-SAD phasing and was refined at 1.89 Å resolution with r.m.s.d. values of 0.009 Å and 1.413° for the bond lengths and angles, respectively. A Ramachandran plot calculated with *PROCHECK* (Laskowski *et al.*, 1993) revealed that 99.7% of the residues are in the most favoured and additionally allowed regions. There were three ABP34 molecules in the asymmetric unit. The three molecules in the asymmetric unit have almost identical conformations, with r.m.s.d. values of 0.54–0.72 Å.

The overall structure of ABP34 is a bent-arm-shaped molecule and the three molecules in the asymmetric unit form a hat-like trimer (Fig. 4*a* and Supplementary Fig. S1). ABP34 adopts a two-domain structure composed of an N-terminal Ca^{2+}-binding domain (N-domain; residues 1–174) and a C-terminal actin-binding domain (C-domain; residues 181–295) (Fig. 4*a*). The two domains are linked by a six-amino-acid loop (175–180). The N-domain is built of eight α-helices (α1–α8), five 3_{10}-helices (η1–η5) and two short β-sheets (β1 and β2). The C-domain contains four α-helices (α9–α12) and one 3_{10}-helix (η6) (Fig. 4*b*). Residues 1–24 and 257–269 could not be built into the final refined model owing to a lack of electron density, implying that the extreme N-terminal region and the loop connecting α11 and α12 are highly flexible. α1 and α2–η1 lie in the same plane, forming a V-shaped turn, and the short α8 perpendicularly penetrates the middle of the opened region of this turn. The resulting triangular structure lies at the border between the EF-hand and the C-domain.

η1 and α3 in the N-domain and α12 in the C-domain are involved in the interdomain interactions, forming a bent-arm-shaped overall ABP34 structure (Figs. 5*a* and 5*b*). The interdomain contact is maintained mainly *via* hydrophobic interactions from η1 and α3 in the N-domain and α12 in the C-domain. Trp54 in η1 and Tyr65 and Trp69 in α3 form a hydrophobic core with Ala273, Trp277 and Trp278 in α12. Phe86 in η3 and the aliphatic region in the side chain of Glu201 in α9 form an additional weak hydrophobic contact away from the hydrophobic core (Fig. 5*a*). The interdomain interactions are further established by hydrogen bonds and electrostatic interactions between the residues in the domain interface (Fig. 5*b*). The interaction pairs are as follows: the backbone carbonyl O atom of Phe86 with the side-chain N^{ε} atom of Arg198, the side-chain carboxyl group of Asp89 with the side-chain guanidinium group of Arg198, the side-chain hydroxyl group of Tyr65 with the side-chain carboxyl group of Asp282, the side-chain carboxyl group of Asn51 with the backbone N atoms of Gly274 and Ala275, and the side-chain imidazole N atom of His177 with the backbone N atom of Gly270 (Fig. 6*b*). In a previous report, the intramolecular interaction between IZ-1 (71–123) and IZ-2 (193–254) was proposed to maintain the N-terminal region (1–76) in close proximity to the strong actin-binding site (193–254) to modulate the interaction of ABP34 with F-actin (Lim, Furukawa & Fechheimer, 1999). Indeed, the hydrophobic and electrostatic interactions of the residues in η3 with its adjacent region (Phe86 and Asp89) and α9 (Arg198 and Glu201) are important for maintaining the overall bent-arm fold and the position of the C-domain of ABP34. There are some possibilities for the disruption of these intermolecular inter-

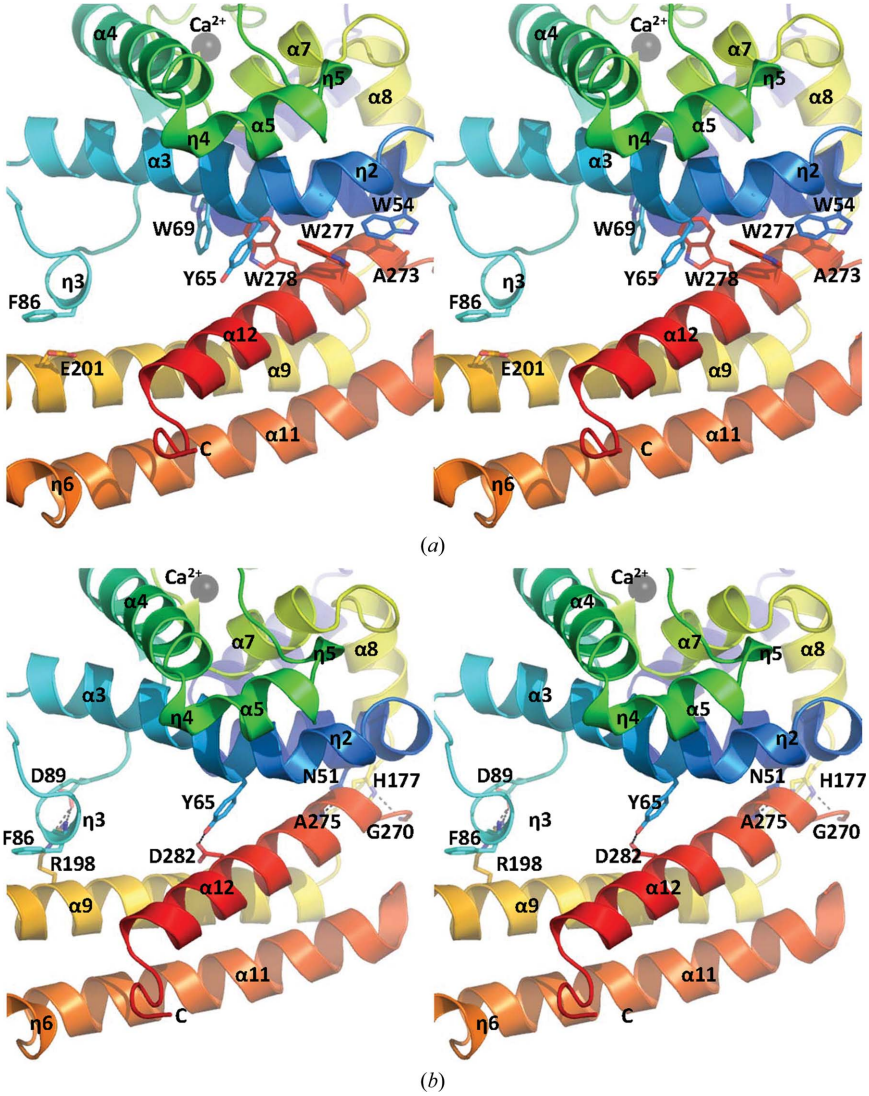

Figure 5
Interdomain interaction. Stereoviews of the interdomain interactions between the N-domain and the C-domain. Side chains which participate in the hydrophobic interactions (*a*) and the electrostatic interactions (*b*) are denoted as sticks and the residue numbers are labelled. The electrostatic interactions are highlighted with black dotted lines. Secondary-structural elements are labelled on the cartoon diagrams. The calcium ion is represented as a black sphere. The overall colour schemes are the same as in Fig. 4.

actions because most interactions are biased towards the linking loop between the N-domain and C-domain. Moreover, the main interdomain interactions of the hydrophobic core have no strong π-stacking interactions among the aromatic side chains.

The N-domain contains one EF-hand motif with bound Ca^{2+} ion. One citrate molecule is located on the noncrystallographic threefold symmetry axis (Supplementary Fig. S1). The only direct interactions among the three ABP34 molecules in the asymmetric unit are the hydrogen bonds between the side-chain hydroxyl group of Tyr101 and the side-chain carboxyl group of Asp144 in an adjacent molecule. The other interactions among the three molecules are formed *via* water molecules and citrate. A structural homologue search using *DALI* (Holm & Rosenström, 2010) revealed that there are 11 hits with a *Z*-score higher than 7.0. The top hit is human PACSIN 1 F-BAR domain (PDB entry 3hai; *Z*-score of 8.3; r.m.s.d. of 2.6 Å over 74 C^{α} atoms; Wang *et al.*, 2009), followed by acriflavine resistance protein A, tubulin-specific chaperone A and SipB (Supplementary Table S1). However, all of the aligned regions of these hits are C-terminal coiled-coil regions in ABP34. Consequently, the overall structure of the full-length ABP34 is a novel fold.

3.5. Calcium-binding N-domain

A calcium ion is important for ABP34 to regulate actin cross-linking (Furukawa *et al.*, 2003). ABP34 is able to cross-link F-actin into bundles in a calcium-regulated manner. ABP34 bundles actin in the presence of a low concentration of calcium (1×10^{-8} *M*), but at elevated calcium levels (1×10^{-6} *M*) the protein is unable to bundle F-actin (Fechheimer, 1987; Fechheimer & Taylor, 1984; Lim & Fechheimer, 1997). The N-domain (1–174) of ABP34 is involved in Ca^{2+} binding and possesses an EF-hand (a helix–loop–helix structural motif), which is typical of many calcium-binding proteins (Kawasaki & Kretsinger, 1994). The EF-hand of ABP34 has a 12-residue Ca^{2+}-binding loop that starts with an aspartate and ends with a glutamate (^{144}DVNFDGRVSFLE^{155}), as found in the canonical EF-hand. The calcium ion is coordinated to amino acids in the segment that includes residues 144–155. Seven oxygen ligands interact with Ca^{2+} with the pattern $X{\bullet}Y{\bullet}Z{\bullet}{-}Y{\bullet}{-}X{\bullet\bullet}{-}Z$, where X, Y, Z, $-Y$, $-X$ and $-Z$ are the ligands that participate in calcium coordination (the monodentate Asp144, Asn146 and Asp148, the main-chain carbonyl group of Arg150, a water molecule and the bidentate Glu155, respectively) and the dots represent intervening residues, forming a pentagonal bipyramidal coordination as found in the canonical EF-hand. The Glu155 residue in the last position of the loop (the $-Z$ ligand) contributes the two O atoms of its γ-carboxyl group (a bidentate ligand). In all known structures of EF-hand proteins, the central residue of the Ca^{2+}-binding loop (the $-Y$ position) binds Ca^{2+} with the main-chain carbonyl O atom (Lewit-Bentley & Réty, 2000; Fig. 6*a*).

The EF-hand is almost always known to occur in pairs, creating a distance of 11 Å between the two bound Ca^{2+} ions (Biekofsky & Feeney, 1998). Stacked with each other in a face-to-face manner, this pair forms a four-helix bundle with the amphipathic helices packed together to make a hydrophobic core. Two EF-hands are further stabilized through a short anti-

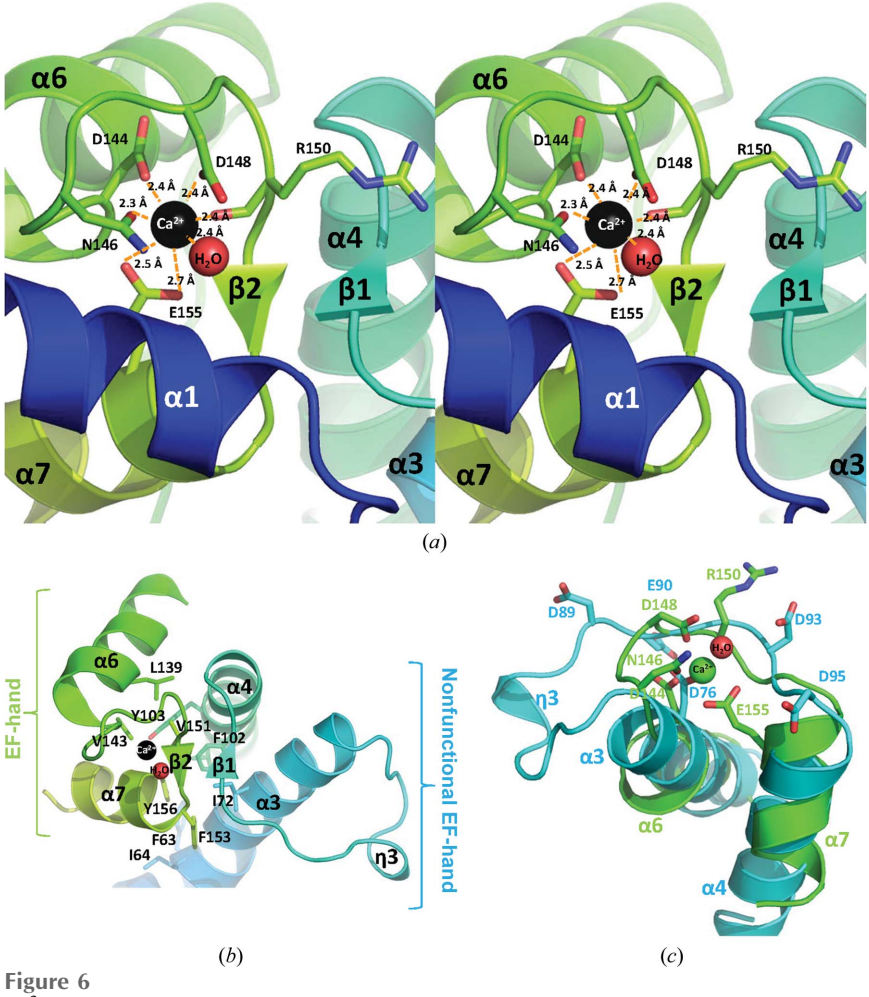

Figure 6
Ca^{2+}-binding N-domain of ABP34. (*a*) Stereo cartoon diagram of the calcium-binding EF-hand in the ABP34 N-domain. Calcium-coordinating ligands from the residues and a water molecule are denoted as sticks and a red sphere, respectively. Secondary-structural elements and the residues are labelled and the calcium ion is indicated by a black sphere. Calcium-coordination interactions are highlighted by orange dotted lines. (*b*) The EF-hand pair in the ABP34 N-domain. The residues are labelled and denoted as sticks. The calcium ion and a water molecule are indicated as black and red spheres, respectively. (*c*) Structural comparison between the EF-hand and the nonfunctional EF-hand in the ABP34 N-domain. All elements in the EF-hand are coloured green except for a water molecule (red), and those in the nonfunctional EF-hand are coloured cyan. The overall colour schemes are same as in Fig. 4.

parallel β-sheet formed between the EF loops of the pairs (Grabarek, 2006). Although the two EF-hands in the domain are related by an approximate twofold axis of symmetry that passes through the eighth position of the loop, they are not identical (Gifford *et al.*, 2007). In ABP34, an EF-hand pair-specific four-helix bundle is formed by the α3, α4, α6 and α7 helices and is maintained by a hydrophobic core (Fig. 6*b*). Two short antiparallel β-sheets (β1 and β2) further stabilize the EF-hand pair. However, the intervening loop between α3 and α4 is composed of 18 amino acids (^{80}KGIQLVFKYDEGNDLDFD^{97}) with one 3_{10}-helix (η3) and one β-sheet (β1). This loop has also lost the proper composition of Ca^{2+}-coordinating ligands. As a result, the putative EF-hand (α3–α4) in ABP34 is not an actual Ca^{2+}-binding site, and this is in accordance with previous reports showing that this putative EF-hand of ABP34 cannot accommodate calcium ion (Maselli *et al.*, 2002; Furukawa *et al.*, 2003; Fig. 6*c*). A nonfunctional EF-hand has also been reported in the case of SCPs (sarcoplasmic Ca^{2+}-binding proteins) from the invertebrate *Nereis diversicolor* (a ragworm). In *Nereis* SCP, although EF2 is nonfunctional owing to an extensive insertion, it is still paired with a functional EF1 and the twofold symmetry is approximately preserved (Vijay-Kumar & Cook, 1992).

The effects of calcium concentration on the conformational change and F-actin-bundling activity of ABP34 may reside in the intramolecular interactions. Previous studies showed that mutations introduced in the EF-hand and the nonfunctional EF-hand cause a loss of the inhibitory effect on F-actin bundling by ABP34 upon an increase in calcium concentration. This is owing to disruption of the function of the first intramolecular interaction zone (IZ-1) in the calcium-binding N-domain of ABP34. The residues in the EF-hand pair (η3, Phe86 and Asp89) are involved in IZ-1 and directly participate in the intramolecular interactions with IZ-2 in the C-domain of ABP34. The defect in IZ-1 may activate actin binding, since the N-terminal calcium-dependent inhibitory region of ABP34 is no longer in close proximity to the strong actin-binding site (ABS2; Lim, Furukawa & Fechheimer, 1999). A concomitant change is that F-actin binding is no longer subject to regulation by calcium binding to the EF-hand. This result suggests that calcium regulation of ABP34 involves a change in the proximity and/or orientation of the N-domain with respect to the strong binding site (ABS2) that is induced by the binding of calcium to the EF-hand. Thus, disruption of the intramolecular interaction in ABP34 not only activates actin binding but also impedes the calcium-dependent regulation of actin binding (Maselli *et al.*, 2002). As a result, the absence or the presence of calcium ion in the EF-hand may affect the stability and/or the conformation of the EF-hand pair and consequently affect the intramolecular interactions between the IZ-1 in the N-domain and the strong actin-binding site (ABS2) in the C-domain. A *DALI* search (Holm & Rosenström, 2010) using the N-domain (1–174) of ABP34 yielded 23 hits covering nine unique proteins with a *Z*-score higher than 6.0. The top hit is calmodulin from *Homo sapiens* (PDB entry 3uct; *Z*-score of 7.2; r.m.s.d. of 1.9 Å over 69 C^{α} atoms; Senguen & Grabarek, 2012), followed by representative EF-hand-containing proteins (S100-A4, calgranulin A, S100-A6, calbindin, troponin C *etc.*) (Supplementary Fig. S4 and Table S2).

3.6. Actin-binding C-domain

ABP34 is known to have three distinct actin-binding sites (ABS) that may contribute to the positive cooperative formation of F-actin bundles [amino acids 1–123 (ABS1), 193–254 (ABS2) and 279–295 (ABS3)], and ABS2 is the strongest actin-binding site (Lim, Furukawa, Eagle *et al.*, 1999; Supplementary Fig. S5). Sequence alignments of ABP34 with other actin-binding proteins revealed that residues 216–244 in ABS2 are conserved in the actin-binding region of α-actinin and ABP120 in *Dictyostelium* (Fig. 7*a*). These conserved sequences are responsible for its binding to actin filaments in α-actinin and ABP120 (Bresnick *et al.*, 1990; Hartwig & Kwiatkowski, 1991) and consist of concentrated hydrophobic and charged amino acids. In addition, hydrophobic interactions are expected to be important in the interaction of filamin (an actin cross-linking protein) and F-actin, and acidic side chains on the actin surface can react with the amino groups in filamin (Djinovic-Carugo & Carugo, 2010).

The three-dimensional structure of the ABP34 C-domain consists of four α-helices (α9–α12), and the C-terminus of α10 is directly followed by one 3_{10}-helix (η6) (Fig. 7*b*). Assuming that the three helices α10, η6 and α11 are part of a long α-helix (α10–η6–α11), α9, α10–η6–α11 and α12 form an antiparallel three-α-helical bundle or left-handed coiled coil with two long helices (α9 and α10–η6–α11) and a shorter C-terminal helix (α12). Helix α9 contains 32 residues (Pro181–Lys212), α10–η6–α11 contains 41 residues (Val216–Gly256) and α12 contains 19 residues (Ser272–Tyr290). Helix α9 is mostly straight, and α10–η6–α11 is disrupted near its midpoint by Gly231 and Pro232, resulting in two α-helices (α10–η6 and α11). The loop between α9 and α10 is very short, with only three residues (^{213}IPG^{215}), whereas the connection between α11 and α12 is five residues in length and is disordered in the crystal structure. The three-helical bundle is maintained by a hydrophobic core encompassing residues Ile183, Ala186, Ala189, Leu190, Val193, Ile197, Leu207 and Thr208 from α9, Ala221 and Leu225 from α10, Ile228 from η6, Leu233, Leu237, Ala240, Leu241, Ala244, Ala247, Val248, Ala251 and Tyr255 from α11 and Ala275, Leu283 and Tyr290 from α12. There are also some polar interactions among the helices: the side-chain carboxyl group of Glu182 with the side-chain amine group of Lys254 and the side-chain hydroxyl group of Tyr255, the side-chain carboxyl group of Asn194 with the side-chain amine group of Lys286, the side-chain hydroxyl group of Tyr200 with the side-chain carboxyl group of Asp229, the side-chain carboxyl group of Glu201 with the side-chain hydroxyl group of Tyr290, the side-chain amine group of Lys234 with the backbone carbonyl O atom of Tyr290, the side-chain carboxyl group of Glu245 with the side-chain amine group of Lys287, and the side-chain hydroxyl group of Ser252 with the side-chain amide group of Asn280.

A *DALI* search (Holm & Rosenström, 2010) using the C-domain (181–295) of ABP34 yielded seven unique proteins

with a *Z*-score higher than 8.0. The top hit is tubulin-binding cofactor A (CoA) from *Leishmania major* (PDB entry 4cqi; *Z*-score of 8.9; r.m.s.d. of 3.6 Å over 87 C^{α} atoms; Barrack *et al.*, 2015), followed by Hsp70, α-spectrin, tubulin-specific chaperone A *etc.* (Supplementary Table S3). Moreover, many of the other low-scoring hits are also included in the rod-shaped helical structure of the spectrin repeats of the cytoskeletal proteins α-actinin, dystrophin and utrophin

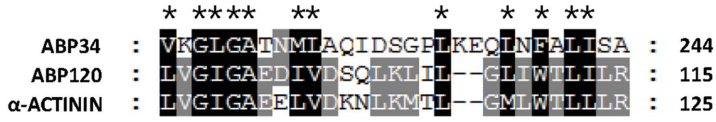

(*a*)

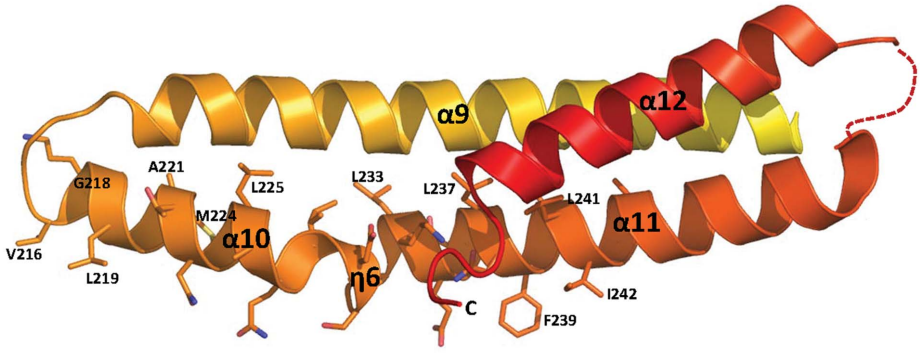

(*b*)

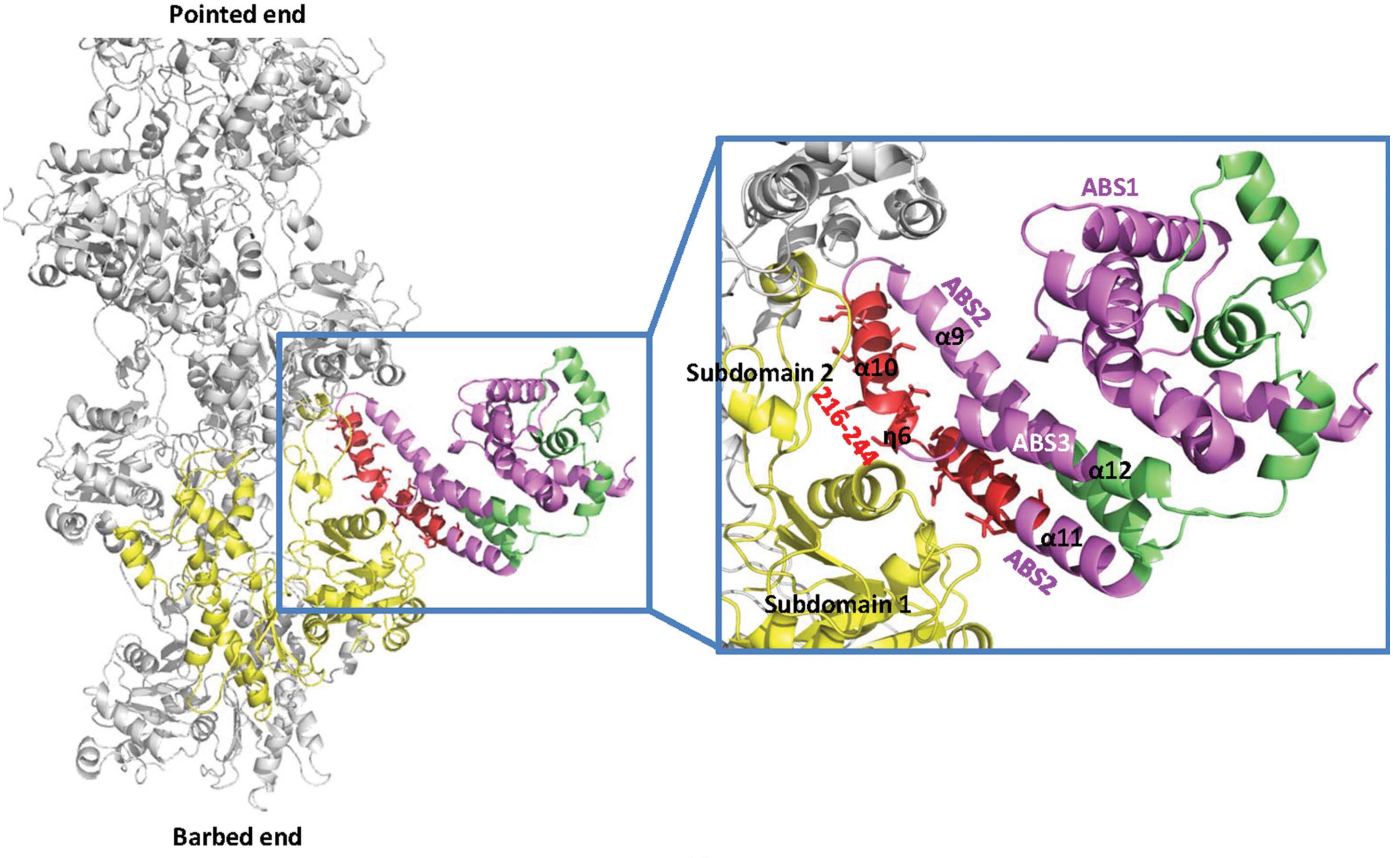

(*c*)

Figure 7
Actin-binding C-domain of ABP34. (*a*) Multiple sequence alignment of the strong actin-binding region (216–244) in the C-domain of ABP34 with the actin-binding regions in α-actinin and ABP120. Conserved residues are highlighted as black boxed letters and are marked with asterisks. (*b*) Cartoon diagram of the ABP34 C-domain. Secondary structures are labelled. Conserved residues in (*a*) are shown as sticks and labelled. The disordered region (257–269) is shown as a dotted line. The overall colour schemes are the same as in Fig. 4. (*c*) Cartoon diagram of the F-actin-binding model. The ABP34 monomer was docked into F-actin using the *PatchDock* server. ABP34 (green) is located on the surface between subdomain 1 and subdomain 2 of an actin monomer (yellow) in F-actin (grey). The conserved strong actin-binding region (216–244) is coloured red and in the enlarged panel residues 216–244 are shown as sticks and the secondary structures in the C-domain are labelled. The three actin-binding sites ABS1, ABS2 and ABS3 are marked and highlighted in magenta.

(Supplementary Fig. S6). These proteins and domains are three-helix bundles or left-handed coiled-coil helical structures, similar to the ABP34 C-terminal domain. This structural homology arises not only because they are both coiled-coil structures, which obviously define a particular fold that can be found in many proteins, but also because the length of the rod units is identical in the ABP34 C-terminal domain and tubulin chaperone cofactor A and spectrin repeats (Guasch *et al.*, 2002). Additionally, the three-helical bundle in the ABP34 C-domain is similar to that of other actin-binding proteins that also have the hydrophobic core formed by bundled folding. It is likely that the three-helical bundle domain stabilizes the conformation of the actin-binding regions. Furthermore, as in the tubulin-binding cofactor A family, the second helix (α10–η6–α11) of the ABP34 C-domain is kinked by a proline break, offering a convex surface towards the solvent area in α10–η6–α11 which is implicated in the strong actin binding (ABS2).

3.7. F-actin-binding model

To gain insights into the F-actin-binding mode of ABP34, molecular docking of F-actin and ABP34 was performed using the *PatchDock* server (Schneidman-Duhovny *et al.*, 2005). The ABP34 monomer was docked into the F-actin structure (PDB entry 3g37; Murakami *et al.*, 2010), and molecular docking was attempted based on the shape-complementary principles algorithm in the *PatchDock* server. After extensive rounds of modelling, we obtained a proper model showing that ABP34 binds to the side of the actin filament and that residues 216–244 in ABS2 fit into a pocket between actin subdomains 1 and 2 with a buried surface (Fig. 7*c*). Actin subdomain 1 (residues 1–32, 70–144 and 338–372) is the preferred target domain for many actin-binding proteins (Djinovic-Carugo & Carugo, 2010). Filamin binds all actin isoforms, and the binding sites on actin have been shown to reside in actin subdomain 1 (Méjean *et al.*, 1992). Moreover, the binding interface between actin and α-actinin is located in actin subdomain 1 near Thr103 (Mimura & Asano, 1987). These sites are also found in other actin-binding proteins, including myosin, tropomyosin and caldesmon (McGough, 1998). As mentioned in §3.6, the conserved residues 216–244 in ABS2 of ABP34 are crucial for strong actin binding and are mostly hydrophobic, which is the force driving the interaction with actin filaments (Franzot *et al.*, 2005). In addition, in cells diverse actin cross-linkers or bundlers interact with the actin filaments by side-binding sequences as in α-actinin (Crevenna *et al.*, 2015). This conserved region is an archetypical binding site for a broad family of actin-binding proteins that bind to the side of actin filaments in the spectrin superfamily, which includes α-actinin and ABP120 (Bresnick *et al.*, 1991; Vandekerckhove & Vancompernolle, 1992; Franzot *et al.*, 2005). Consequently, residues 216–244 of ABP34 may bind to the side of subdomain 1 in an actin filament through hydrophobic interaction between the surface residues on ABS2, similarly to several other actin-bundling proteins.

ABP34 has three actin-binding sites (ABS1, ABS2 and ABS3) and induces the formation of the most highly ordered bundles with short centre-to-centre spacing of actin filaments (Furukawa & Fechheimer, 1990). Thus, the three actin-binding sites may interact with F-actin filaments as a compact monomeric form (Lim, Furukawa & Fechheimer, 1999). Similarly, two ABDs (ABD1 and ABD2) of fimbrin are tandemly arranged on the same polypeptide and bundled the actin into tightly packed filaments as a monomer (Hanein *et al.*, 1998). Moreover, fascin also binds actin as monomer and contains two major actin-binding sites (Jansen *et al.*, 2011). The actin-binding sites of fascin are conformationally interconnected. Hence, it is likely that the binding of one F-actin filament at one actin-binding site stabilizes fascin in the active configuration and enhances the binding of actin filaments at the other actin-binding sites (Yang *et al.*, 2013). In ABP34, the second and third actin-binding sites, ABS2 and ABS3, bind to one actin filament by hydrophobic and positive charged residues, respectively, and the other actin filament may be bound to ABS1 in the N-domain by positively charged amino-acid residues (Fechheimer *et al.*, 1991). As mentioned in §3.5, bivalent F-actin binding of ABP34 may be regulated by the intramolecular interactions depending on the concentration of calcium ion and the stability/conformation of the EF-hand pair which is involved in the N-terminal actin-binding site (ABS1). Additionally, F-actin at one end might induce a direct conformational change at the opposing end of ABP34 that could alter its binding affinity for F-actin, resulting in cooperative binding that could explain its unique ability to form tightly packed and ordered actin bundles (Sedeh *et al.*, 2010) as in the case of fascin.

4. Conclusion

ABP34 is a calcium-regulated 34 kDa F-actin-bundling protein from *D. discoideum*. The F-actin-binding and F-actin-bundling activities of recombinant ABP34 were verified by a co-sedimentation assay and transmission electron-microscopy data, respectively. The co-localization of ABP34 and actin in cells was also confirmed through fluorescence microscopy. The 1.89 Å resolution crystal structure of ABP34 solved by Ca^{2+}/S-SAD revealed that ABP34 adopts a two-domain structure with an EF-hand-containing N-domain and a strong actin-binding C-domain. The EF-hand is occupied by a calcium ion with pentagonal bipyramidal coordination as in the canonical EF-hand. The C-domain is a three-helical bundle that superposes well onto the rod-shaped helical structures of some cytoskeletal proteins. Residues 216–244 in the C-domain are part of the strongest actin-binding sites (193–254) and have conserved sequences with the actin-binding regions of α-actinin and ABP120. The second helical region of the C-domain is kinked by a proline break, offering a convex surface towards the solvent area which is implicated in actin binding. The F-actin-binding model suggests that ABP34 may bind to the side of actin and that residues 216–244 fit into a pocket between actin subdomains 1 and 2 through hydrophobic interactions. The interdomain interactions not only maintain the overall bent-arm-shaped fold, but also participate in the connection between calcium binding (the EF-hand

in the N-domain) and actin binding (ABS2 in the C-domain). To elucidate the detailed mechanism through which ABP34 achieves F-actin bundling in a calcium-regulated manner, it is essential to obtain the crystal structures of Ca^{2+}-free ABP34 and the actin complex of ABP34; these efforts are ongoing.

5. Related literature

The following references are cited in the Supporting Information for this article: Akama *et al.* (2004), Arbing *et al.* (2013), Barta *et al.* (2012), Biou *et al.* (1994), Boudko *et al.* (2007), Crespillo *et al.* (2014), Duelli *et al.* (2014), Grum *et al.* (1999), Henne *et al.* (2007), Itou *et al.* (2002), Korndörfer *et al.*, 2007), Li *et al.* (2006), Lu *et al.* (2010), Macias *et al.* (2011), Mäler *et al.* (2000), Mikolosko *et al.* (2006), Otterbein *et al.* (2002), Partha *et al.* (2014), Plomann *et al.* (2010), Ray *et al.* (2003), Senguen & Grabarek (2012), Sondermann *et al.* (2001), Vassylyev *et al.* (1998), Wang *et al.* (2009) and Williamson *et al.* (2009).

Acknowledgements

We thank the beamline staff at BL-6C and BL-7A, PLS, Republic of Korea for support with the data collection. We thank Dr Sun-Shin Cha at KIOST for his valuable advice. This study was supported by a BK21 Plus Research Fellowship from the Ministry of Education, Science and Technology, Republic of Korea.

References

Adams, P. D. *et al.* (2010). *Acta Cryst.* D**66**, 213–221.
Akama, H., Kanemaki, M., Yoshimura, M., Tsukihara, T., Kashiwagi, T., Yoneyama, H., Narita, S., Nakagawa, A. & Nakae, T. (2004). *J. Biol. Chem.* **279**, 52816–52819.
Anderson, C. M., McDonald, R. C. & Steitz, T. A. (1978). *J. Mol. Biol.* **123**, 1–13.
Arbing, M. A., Chan, S., Harris, L., Kuo, E., Zhou, T. T., Ahn, C. J., Nguyen, L., He, Q., Lu, J., Menchavez, P. T., Shin, A., Holton, T., Sawaya, M. R., Cascio, D. & Eisenberg, D. (2013). *PLoS One*, **8**, e81753.
Barrack, K. L., Fyfe, P. K. & Hunter, W. N. (2015). *Acta Cryst.* F**71**, 539–546.
Barta, M. L., Dickenson, N. E., Patil, M., Keightley, A., Wyckoff, G. J., Picking, W. D., Picking, W. L. & Geisbrecht, B. V. (2012). *J. Mol. Biol.* **417**, 395–405.
Biekofsky, R. R. & Feeney, J. (1998). *FEBS Lett.* **439**, 101–106.
Biou, V., Yaremchuk, A., Tukalo, M. & Cusack, S. (1994). *Science*, **263**, 1404–1410.
Bork, P., Sander, C. & Valencia, A. (1992). *Proc. Natl Acad. Sci. USA*, **89**, 7290–7294.
Boudko, S. P., Kuhn, R. J. & Rossmann, M. G. (2007). *J. Mol. Biol.* **366**, 1538–1544.
Bresnick, A. R., Janmey, P. A. & Condeelis, J. (1991). *J. Biol. Chem.* **266**, 12989–12993.
Bresnick, A. R., Warren, V. & Condeelis, J. (1990). *J. Biol. Chem.* **265**, 9236–9240.
Broderick, M. J. & Winder, S. J. (2005). *Adv. Protein Chem.* **70**, 203–246.
Crespillo, S., Cámara-Artigas, A., Casares, S., Morel, B., Cobos, E. S., Mateo, P. L., Mouz, N., Martin, C. E., Roger, M. G., El Habib, R., Su, B., Moog, C. & Conejero-Lara, F. (2014). *Proc. Natl Acad. Sci. USA*, **111**, 18207–18212.
Crevenna, A. H., Arciniega, M., Dupont, A., Mizuno, N., Kowalska, K., Lange, O. F., Wedlich-Soldner, R. & Lamb, D. C. (2015). *Elife*, **4**, e04599.
Derman, A. I., Becker, E. C., Truong, B. D., Fujioka, A., Tucey, T. M., Erb, M. L., Patterson, P. C. & Pogliano, J. (2009). *Mol. Microbiol.* **73**, 534–552.
Djinovic-Carugo, K. & Carugo, O. (2010). *Curr. Protein Pept. Sci.* **11**, 639–650.
Duelli, A., Kiss, B., Lundholm, I., Bodor, A., Petoukhov, M. V., Svergun, D. I., Nyitray, L. & Katona, G. (2014). *PLoS One*, **9**, e97654.
Emsley, P. & Cowtan, K. (2004). *Acta Cryst.* D**60**, 2126–2132.
van den Ent, F., Amos, L. A. & Löwe, J. (2001). *Nature (London)*, **413**, 39–44.
van den Ent, F. & Löwe, J. (2000). *EMBO J.* **19**, 5300–5307.
van den Ent, F., Møller-Jensen, J., Amos, L. A., Gerdes, K. & Löwe, J. (2002). *EMBO J.* **21**, 6935–6943.
Ettema, T. J., Lindås, A. C. & Bernander, R. (2011). *Mol. Microbiol.* **80**, 1052–1061.
Fechheimer, M. (1987). *J. Cell Biol.* **104**, 1539–1551.
Fechheimer, M. & Furukawa, R. (1991). *Methods Enzymol.* **196**, 84–91.
Fechheimer, M., Ingalls, H. M., Furukawa, R. & Luna, E. J. (1994). *J. Cell Sci.* **107**, 2393–2401.
Fechheimer, M., Murdock, D., Carney, M. & Glover, C. V. (1991). *J. Biol. Chem.* **266**, 2883–2889.
Fechheimer, M. & Taylor, D. L. (1984). *J. Biol. Chem.* **259**, 4514–4520.
Flaherty, K. M., DeLuca-Flaherty, C. & McKay, D. B. (1990). *Nature (London)*, **346**, 623–628.
Franzot, G., Sjöblom, B., Gautel, M. & Djinović Carugo, K. (2005). *J. Mol. Biol.* **348**, 151–165.
Furukawa, R., Butz, S., Fleischmann, E. & Fechheimer, M. (1992). *Protoplasma*, **169**, 18–27.
Furukawa, R. & Fechheimer, M. (1990). *Dev. Genet.* **11**, 362–368.
Furukawa, R. & Fechheimer, M. (1994). *Cell Motil. Cytoskeleton*, **29**, 46–56.
Furukawa, R. & Fechheimer, M. (1997). *Int. Rev. Cytol.* **175**, 29–90.
Furukawa, R., Maselli, A., Thomson, S. A. M., Lim, R. W. L., Stokes, J. V. & Fechheimer, M. (2003). *J. Cell Sci.* **116**, 187–196.
Gifford, J. L., Walsh, M. P. & Vogel, H. J. (2007). *Biochem. J.* **405**, 199–221.
Gimona, M., Djinovic-Carugo, K., Kranewitter, W. J. & Winder, S. J. (2002). *FEBS Lett.* **513**, 98–106.
Goodson, H. V. & Hawse, W. F. (2002). *J. Cell Sci.* **115**, 2619–2622.
Grabarek, Z. (2006). *J. Mol. Biol.* **359**, 509–525.
Grosse-Kunstleve, R. W. & Adams, P. D. (2003). *Acta Cryst.* D**59**, 1966–1973.
Grum, V. L., Li, D., MacDonald, R. I. & Mondragón, A. (1999). *Cell*, **98**, 523–535.
Guasch, A., Aloria, K., Pérez, R., Avila, J., Zabala, J. C. & Coll, M. (2002). *J. Mol. Biol.* **318**, 1139–1149.
Hanein, D., Volkmann, N., Goldsmith, S., Michon, A. M., Lehman, W., Craig, R., DeRosier, D., Almo, S. & Matsudaira, P. (1998). *Nature Struct. Biol.* **5**, 787–792.
Hartwig, J. H. & Kwiatkowski, D. J. (1991). *Curr. Opin. Cell Biol.* **3**, 87–97.
Henne, W. M., Kent, H. M., Ford, M. G., Hegde, B. G., Daumke, O., Butler, P. J., Mittal, R., Langen, R., Evans, P. R. & McMahon, H. T. (2007). *Structure*, **15**, 839–852.
Holm, L. & Rosenström, P. (2010). *Nucleic Acids Res.* **38**, W545–W549.
Hurley, J. H., Faber, H. R., Worthylake, D., Meadow, N. D., Roseman, S., Pettigrew, D. W. & Remington, S. J. (1993). *Science*, **259**, 673–677.
Itou, H., Yao, M., Fujita, I., Watanabe, N., Suzuki, M., Nishihira, J. & Tanaka, I. (2002). *J. Mol. Biol.* **316**, 265–276.
Jansen, S., Collins, A., Yang, C., Rebowski, G., Svitkina, T. & Dominguez, R. (2011). *J. Biol. Chem.* **286**, 30087–30096.

Johns, J. A., Brock, A. M. & Pardee, J. D. (1988). *Cell Motil. Cytoskeleton*, **9**, 205–218.
Jones, T. A., Zou, J.-Y., Cowan, S. W. & Kjeldgaard, M. (1991). *Acta Cryst.* A**47**, 110–119.
Kabsch, W. & Holmes, K. C. (1995). *FASEB J.* **9**, 167–174.
Kawasaki, H. & Kretsinger, R. H. (1994). *Protein Profile*, **1**, 343–517.
Kim, J.-S., Seo, J.-H., Yim, H.-S. & Kang, S.-O. (2011). *FEBS Lett.* **585**, 1864–1872.
Koch, M., Diez, J., Wagner, A. & Fritz, G. (2010). *Acta Cryst.* F**66**, 1032–1036.
Komeili, A., Li, Z., Newman, D. K. & Jensen, G. J. (2006). *Science*, **311**, 242–245.
Korndörfer, I. P., Brueckner, F. & Skerra, A. (2007). *J. Mol. Biol.* **370**, 887–898.
Laskowski, R. A., Moss, D. S. & Thornton, J. M. (1993). *J. Mol. Biol.* **231**, 1049–1067.
Lee, C.-H., Jeong, S.-Y., Kim, B.-J., Choi, C.-H., Kim, J.-S., Koo, B.-M., Seok, Y.-J., Yim, H.-S. & Kang, S.-O. (2005). *Biochim. Biophys. Acta*, **1743**, 281–290.
Lewit-Bentley, A. & Réty, S. (2000). *Curr. Opin. Struct. Biol.* **10**, 637–643.
Li, S., Sandercock, A. M., Conduit, P., Robinson, C. V., Williams, R. L. & Kilmartin, J. V. (2006). *J. Cell Biol.* **173**, 867–877.
Lim, R. W. L. & Fechheimer, M. (1997). *Protein Expr. Purif.* **9**, 182–190.
Lim, R. W. L., Furukawa, R., Eagle, S., Cartwright, R. C. & Fechheimer, M. (1999). *Biochemistry*, **38**, 800–812.
Lim, R. W. L., Furukawa, R. & Fechheimer, M. (1999). *Biochemistry*, **38**, 16323–16332.
Lindås, A.-C., Chruszcz, M., Bernander, R. & Valegård, K. (2014). *Acta Cryst.* D**70**, 492–500.
Lu, L., Nan, J., Mi, W., Li, L.-F., Wei, C.-H., Su, X.-D. & Li, Y. (2010). *FEBS Lett.* **584**, 3533–3539.
Macias, A. T. *et al.* (2011). *J. Med. Chem.* **54**, 4034–4041.
Mäler, L., Blankenship, J., Rance, M. & Chazin, W. J. (2000). *Nature Struct. Biol.* **7**, 245–250.
Maselli, A. G., Davis, R., Furukawa, R. & Fechheimer, M. (2002). *J. Cell Sci.* **115**, 1939–1949.
Matsudaira, P. (1991). *Trends Biochem. Sci.* **16**, 87–92.
Matthews, B. W. (1968). *J. Mol. Biol.* **33**, 491–497.
McCoy, A. J., Grosse-Kunstleve, R. W., Adams, P. D., Winn, M. D., Storoni, L. C. & Read, R. J. (2007). *J. Appl. Cryst.* **40**, 658–674.
McGough, A. (1998). *Curr. Opin. Struct. Biol.* **8**, 166–176.
Méjean, C., Lebart, M.-C., Boyer, M., Roustan, C. & Benyamin, Y. (1992). *Eur. J. Biochem.* **209**, 555–562.
Mikolosko, J., Bobyk, K., Zgurskaya, H. I. & Ghosh, P. (2006). *Structure*, **14**, 577–587.
Mimura, N. & Asano, A. (1987). *J. Biol. Chem.* **262**, 4717–4723.
Murakami, K., Yasunaga, T., Noguchi, T. Q. P., Gomibuchi, Y., Ngo, K. X., Uyeda, T. Q. P. & Wakabayashi, T. (2010). *Cell*, **143**, 275–287.
Murshudov, G. N., Skubák, P., Lebedev, A. A., Pannu, N. S., Steiner, R. A., Nicholls, R. A., Winn, M. D., Long, F. & Vagin, A. A. (2011). *Acta Cryst.* D**67**, 355–367.
Noegel, A. A. & Luna, J. E. (1995). *Experientia*, **51**, 1135–1143.
Okazaki, K. & Yumura, S. (1995). *Eur. J. Cell Biol.* **66**, 75–81.
Otterbein, L. R., Kordowska, J., Witte-Hoffmann, C., Wang, C. L. & Dominguez, R. (2002). *Structure*, **10**, 557–567.
Otto, J. J. (1994). *Curr. Opin. Cell Biol.* **6**, 105–109.
Otwinowski, Z. & Minor, W. (1997). *Methods Enzymol.* **276**, 307–326.
Partha, S. K., Ravulapalli, R., Allingham, J. S., Campbell, R. L. & Davies, P. L. (2014). *FEBS J.* **281**, 3138–3149.
Plomann, M., Wittmann, J. G. & Rudolph, M. G. (2010). *J. Mol. Biol.* **400**, 129–136.
Prassler, J., Stocker, S., Marriott, G., Heidecker, M., Kellermann, J. & Gerisch, G. (1997). *Mol. Biol. Cell*, **8**, 83–95.
Ramagopal, U. A., Dauter, M. & Dauter, Z. (2003). *Acta Cryst.* D**59**, 868–875.
Ray, S. S., Bonanno, J. B., Chen, H., de Lencastre, H., Wu, S., Tomasz, A. & Burley, S. K. (2003). *Proteins*, **50**, 170–173.
Roeser, D., Dickmanns, A., Gasow, K. & Rudolph, M. G. (2005). *Acta Cryst.* D**61**, 1057–1066.
Schleicher, M. & Noegel, A. A. (1992). *New Biol.* **4**, 461–472.
Schneidman-Duhovny, D., Inbar, Y., Nussinov, R. & Wolfson, H. J. (2005). *Nucleic Acids Res.* **33**, W363–W367.
Sedeh, R. S., Fedorov, A. A., Fedorov, E. V., Ono, S., Matsumura, F., Almo, S. C. & Bathe, M. (2010). *J. Mol. Biol.* **400**, 589–604.
Senguen, F. T. & Grabarek, Z. (2012). *Biochemistry*, **51**, 6182–6194.
Sheldrick, G. M. (2010). *Acta Cryst.* D**66**, 479–485.
Sondermann, H., Scheufler, C., Schneider, C., Hohfeld, J., Hartl, F.-U. & Moarefi, I. (2001). *Science*, **291**, 1553–1557.
Terwilliger, T. C. (2002). *Acta Cryst.* D**58**, 1937–1940.
Terwilliger, T. C., Adams, P. D., Read, R. J., McCoy, A. J., Moriarty, N. W., Grosse-Kunstleve, R. W., Afonine, P. V., Zwart, P. H. & Hung, L.-W. (2009). *Acta Cryst.* D**65**, 582–601.
Vandekerckhove, J. & Vancompernolle, K. (1992). *Curr. Opin. Cell Biol.* **4**, 36–42.
Vassylyev, D. G., Takeda, S., Wakatsuki, S., Maeda, K. & Maéda, Y. (1998). *Proc. Natl Acad. Sci. USA*, **95**, 4847–4852.
Vijay-Kumar, S. & Cook, W. J. (1992). *J. Mol. Biol.* **224**, 413–426.
Vorobiev, S., Strokopytov, B., Drubin, D. G., Frieden, C., Ono, S., Condeelis, J., Rubenstein, P. A. & Almo, S. C. (2003). *Proc. Natl Acad. Sci. USA*, **100**, 5760–5765.
Wang, Q., Navarro, M. V. A. S., Peng, G., Molinelli, E., Lin Goh, S., Judson, B. L., Rajashankar, K. R. & Sondermann, H. (2009). *Proc. Natl Acad. Sci. USA*, **106**, 12700–12705.
Williamson, D. S. *et al.* (2009). *J. Med. Chem.* **52**, 1510–1513.
Yang, S., Huang, F.-K., Huang, J., Chen, S., Jakoncic, J., Leo-Macias, A., Diaz-Avalos, R., Chen, L., Zhang, J. J. & Huang, X.-Y. (2013). *J. Biol. Chem.* **288**, 274–284.